
Disclaimer

This manuscript has been submitted to NATURE COMMUNICATIONS EARTH & ENVIRONMENT, and is not peer-reviewed.

Please feel free to contact any of the authors with feedback and suggestions for improvements.

Document history

Date	Action
03/Aug/2022	MS sent to co-authors for final draft acceptance Supplementary materials uploaded to Zenodo MS Submitted to EarthArXiv MS Submitted to Communications Earth and Environment

THE INFLUENCE OF REEF ISOSTASY, DYNAMIC TOPOGRAPHY, AND GLACIAL ISOSTATIC ADJUSTMENT ON THE LAST INTERGLACIAL SEA-LEVEL RECORD OF NORTHEASTERN AUSTRALIA.

PREPRINT, COMPILED AUGUST 3, 2022

Alessio Rovere^{1,2*}, Tamara Pico³, Frederick Richards⁴, Michael J. O'Leary⁵, Jerry X. Mitrovica⁶, Ian D. Goodwin^{7,8}, Jacqueline Austermann⁹, and Konstantin Latychev⁶

¹Department of Environmental Sciences, Informatics and Statistics, Ca' Foscari University of Venice, IT

²MARUM - Center for Marine Environmental Sciences, University of Bremen, DE Germany

³Earth & Planetary Sciences Department, UC Santa Cruz, Santa Cruz, USA

⁴Department of Earth Science & Engineering, Imperial College London, London, UK

⁵School of Earth Sciences, University of Western Australia Oceans Institute, Perth, AU

⁶Department of Earth and Planetary Sciences, Harvard University, Boston, USA

⁷Climalab, New South Wales, AU

⁸Climate Change Research Centre and Australian Centre for Excellence in Antarctic Science, University of New South Wales, AU

⁹Department of Earth and Environmental Sciences & Lamont-Doherty Earth Observatory, Columbia University, New York, USA

ABSTRACT

NOTE FOR THE READER: this is a preprint of a manuscript submitted to Nature Communications Earth & Environment. This manuscript has not been peer-reviewed.

Understanding sea level during the warmest peak of the Last Interglacial (125,000 yrs ago; Marine Isotope Stage 5e) is important for assessing future ice-sheet dynamics in response to climate change, and relies on the measurement and interpretation of paleo sea-level indicators, corrected for post-depositional vertical land motions. The coasts and continental shelves of northeastern Australia (Queensland) preserve an extensive Last Interglacial record in the facies of coastal strandplains onland and fossil reefs offshore. However, there is a discrepancy (amounting to tens of meters) in the elevation of sea-level indicators between offshore and onshore sites. Here, we assess the influence of geophysical processes that may have changed the elevation of these sea-level indicators since the Last Interglacial. We modeled sea-level change due to: i) dynamic topography; ii) glacial isostatic adjustment, and iii) isostatic adjustment due to coral reef loading, which we term "reef isostasy". These processes caused relative sea-level changes on the order of, respectively, 10 m, 5 m, and 0.3 m since the Last Interglacial. Of these geophysical processes, the dynamic topography predictions most closely match the tilting observed between onshore and offshore sea-level markers. However, we found that these combined geophysical processes cannot explain the full amplitude of the observed discrepancy between onshore and offshore sea-level indicators.

Keywords Last Interglacial · Sea level changes · NE Australia · Great Barrier Reef

INTRODUCTION

Reef coring typically encountered LIG reefs between 5 and 20 m below the modern GBR reef flats. Strikingly, along the Queensland and far northern New South Wales coastline, LIG strandplains are identified at higher elevations with ridge/swale heights (ranging from +3 to +9m) than offshore LIG reefs [60, 33]. These onshore markers are not as precisely dated as the coral sea-level markers, however they were arguably formed during the LIG. The higher elevations of these coastal strandplains are roughly consistent with estimates for peak LIG global mean sea level (GMSL). Such estimates are consistently above modern mean sea level (0 m), albeit they vary substantially depending on study sites analyzed and corrections for vertical land motions applied to the proxy record (from 6 to 9 m [43], 8 m [23], 2 m [78], and 1-5 m [24]).

The most obvious explanation of the discrepancy between onshore and offshore LIG sea-level indicators in Northeastern Australia is that these two areas are subject to differential vertical land motions. When reconstructing past global mean sea

level (GMSL) from geological sea-level proxies, it is essential to disentangle the components causing globally averaged sea-level changes from other regional processes that may have caused vertical displacement of past sea-level indicators [65, 69]. Among these, the most relevant are glacial isostatic adjustment (GIA) [25], tectonic deformation processes [54] and mantle dynamic topography (DT) [5].

Crustal loading due to local processes can also cause the vertical displacement of observed sea-level indicators through isostatic adjustment. For example, sediment loading can cause regional sea level to depart significantly from the global mean along major deltaic systems [18, 64, 27, 64, 71, 26, 88]. Karst erosion is another mechanism that induces isostatic adjustment, through mass unloading, causing a net crustal uplift. This process is represented in the Plio-Pleistocene shoreline complexes in Florida, that were uplifted following isostatic response to the karstification (leading to rock mass loss) of the landscape [16, 61, 1, 89]. To date, estimates of peak LIG GMSL from tropical areas have not accounted for the isostatic response to coral reef loading

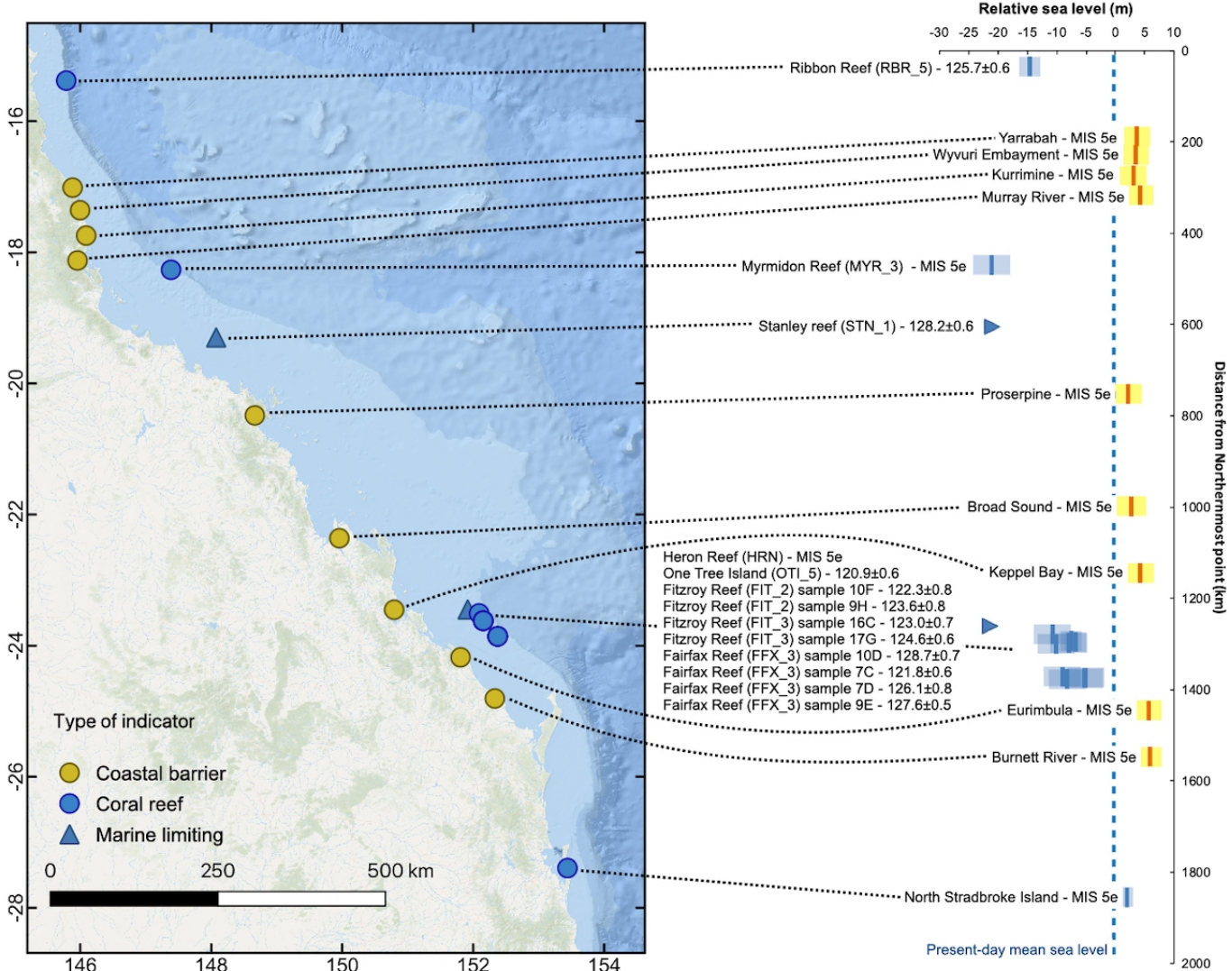


Figure 1: Map (left panel) and elevation plot (right panel) of LIG paleo RSL obtained from fossil reefs (blue markers) and beach barriers (yellow markers) along the GBR and the Queensland Coasts. Error bars represent 1-sigma ranges.

over the last glacial cycle. This process stems from the fact that corals can grow into spatially extensive reefs, reaching thicknesses of several tens of meters during interglacials. The effect of reef accretion and related loading on local sea-level histories remains largely unexplored.

In this work, we model the influence of geophysical processes that may have changed the elevation of geologic sea-level indicators along the Queensland coasts and offshore, on the GBR, since the LIG. We assess the extent to which the combined geophysical processes of glacial isostatic adjustment and dynamic topography may have impacted the LIG sea-level record in this region. Importantly, in this study we also isolate the process of coral reef loading, and assess its importance in causing regional departures from GMSL. While we find that the combined geophysical processes modeled in this study cannot fully explain the amplitude of the observed discrepancy between onshore and offshore sea-level markers in the study area, we identify

that dynamic topography may represent the key to solve this conundrum.

1 LIG SEA-LEVEL INDICATORS

The study of past sea-level changes relies on the measurement and dating of relative sea-level (RSL) indicators, i.e. geological proxies that formed in connection with former positions of the sea. Once a sea-level indicator is measured and dated, it is necessary to establish its indicative meaning [84, 76] to quantify the relationship between the elevation or depth of an indicator and the position of the former sea level, including associated uncertainties due to the environmental range of formation. Once the elevation of a sea-level indicator is corrected, taking into account its indicative meaning, it reflects paleo relative sea level (RSL), i.e., the paleo position of the sea including both barystatic (i.e., eustatic, 35) changes and elevation changes due to vertical land motions of different origin.

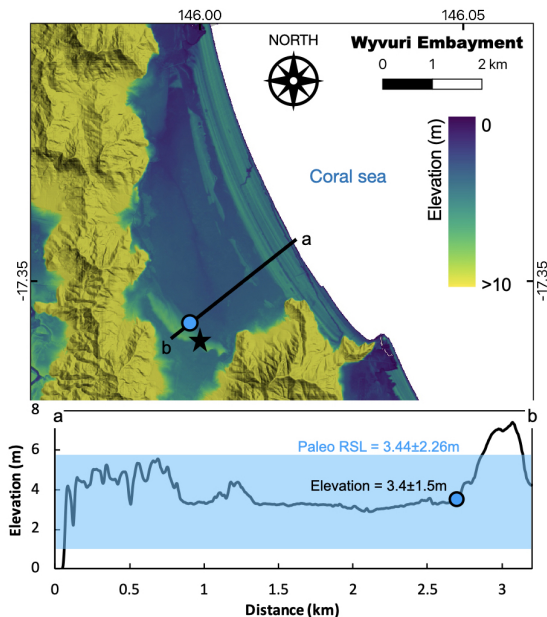


Figure 2: Digital Elevation Model [31] and topographic profile (a-b) of the Wyvuri Embayment, where [30] identified LIG coastal sediments in a core under a dune/beach barrier. The star indicates the approximate point where core JW4 of [30] was drilled. The blue dot indicates the inner part of the LIG barrier, that was used as a sea-level proxy in this study. The blue transparent overlay indicates the paleo RSL calculated using the elevation of the inner margin of the barrier and the indicative meaning calculator tool [52].

ogy for these strandplains is in progress [33], and shows that complete LIG strandplains are located inboard of the modern Holocene equivalents. In far north Queensland, Gagan et al. [30] describes a LIG dune/beach barrier located onshore with respect to the Holocene equivalent at Wyvuri Embayment (Figure 2). The top of the barrier, composed of aeolian sediments, is located at +6 m above modern sea-level, while the beach barrier sands were intercepted about 4 meters below the surface, in drill cores. This elevation roughly corresponds to a break in slope on the coastal plain (3.4 ± 1.5 m), which can be interpreted as a shoreline angle. Considering this a beach deposit, and using the indicative meaning calculator [52], we calculate that this strandplain indicates a LIG paleo RSL of 3.44 ± 2.26 m (Figure 2). At the nearby Cowley Beach strandplain, Brooke et al. [9] established that the strandplain beach ridge morphology tracked Holocene sea-level trends.

The surface expression of the Wyvuri Embayment LIG beach barrier can be found at other locations along the Queensland coast, with the shoreline angle located roughly at the same elevation as that of Wyvury Embayment (yellow markers in Figure 1).

Starting from the description of Gagan et al. [30] and high-resolution (5m) Digital Elevation Models from [31], we identified other locations scattered along the Queensland coast where the LIG beach barrier is visible and where sea-level index points can be derived (see Supplementary Materials for detailed maps of each area and a spreadsheet containing sea-level interpretations, similar to those shown in Figure 2). The elevation of these barriers is consistent with those identified in northern New South Wales, which preserve a LIG sea-level trend from a highstand at $+6 \pm 0.5$ m at 129 ka BP to $+4$ m by 116 ka BP [33]. The SE Queensland and northern New South Wales studies revealed that regional coastal fault reactivation has occurred during the Late Quaternary that has influenced the accommodation space for strandplain deposition. Overall the Late Quaternary onshore strandplains extending from far North Queensland to far northern New South Wales records indicate that the coastline and relative sea-levels since MIS 7 are preserved in the $+3$ to $+6$ m elevation. This is in stark contrast to the offshore submerged record, suggesting a LIG paleo relative sea level below the modern one.

The fact that LIG reefs in the GBR are found below the typical elevation of reefs of the same age on passive continental margins was discussed by [53], who attributed it to a combination of long-term subsidence of the continental margin and erosion of the Pleistocene reef framework during glacial times. Differential Holocene reef growth rates seem to indicate that the Central GBR is subsiding with respect to the Northern and Southern GBR [20], and this subsidence may be related to the re-activation of NNW-SSE extensional faults along the eastern Queensland margin [73, and references therein].

2 REEF ISOSTASY

Coral reefs are created by the fixation of calcium carbonate mostly by hermatypic corals and calcareous algae [90], that respond to variations in sea-level by catching up, keeping up or giving up. From the geological perspective, this results in the creation of a mass of reef framework, which can exert a

72 On the GBR, corals of LIG age are presently preserved under
 73 a subsurface unconformity, which occurs between 3-5 to 20-25
 74 meters below present sea level, depending on the site [39, 53, 72].
 75 Murray-Wallace and Belperio [60] highlight that, while low-
 76 lying islands are scattered throughout the GBR, outcrops of
 77 Pleistocene reefs above modern sea level are absent. The only
 78 exception may be an exposed reef of supposed Pleistocene age
 79 at 1-4m above present sea level [39] at Digby Island [47, 48].
 80 However, the age of this reef has never been confirmed with
 81 absolute dating, and it will not be discussed further. Retrieval
 82 of LIG reef sections on the GBR has been historically done by
 83 coring through the Holocene reef down to the Holocene/LIG un-
 84 conformity. A full account of the best-preserved and best-dated
 85 Last Interglacial corals on the GBR, alongside their indicative
 86 meaning, is provided by Dechnik et al. [19]. These data were
 87 recently compiled into the standardized WALIS (World Atlas
 88 of Last Interglacial Shorelines) database by Chutcharavan and
 89 Dutton [15] (blue markers in Figure 1)

90 Murray-Wallace and Belperio [60] report the presence of scat-
 91 tered coastal deposits of LIG age along the continental coasts
 92 of Queensland. These deposits become ubiquitous along the
 93 SE Queensland Fraser Island Coast and far north New South
 94 Wales coasts [33]. In contrast to LIG reef sequences in the GBR,
 95 most of these strandplains are rarely assigned an age with abso-
 96 lute dating techniques. Their MIS 5e age has been inferred via
 97 chronostratigraphic correlation with lower younger (Holocene)
 98 units, and infinite radiocarbon ages. An expanding OSL chronol-

99
 100
 101
 102
 103
 104
 105
 106
 107
 108
 109
 110
 111
 112
 113
 114

115
 116
 117
 118
 119

120
 121
 122
 123
 124
 125
 126
 127
 128
 129
 130

131
 132
 133
 134
 135
 136
 137
 138
 139

140
 141
 142
 143
 144
 145
 146
 147
 148
 149

150
 151
 152
 153
 154
 155

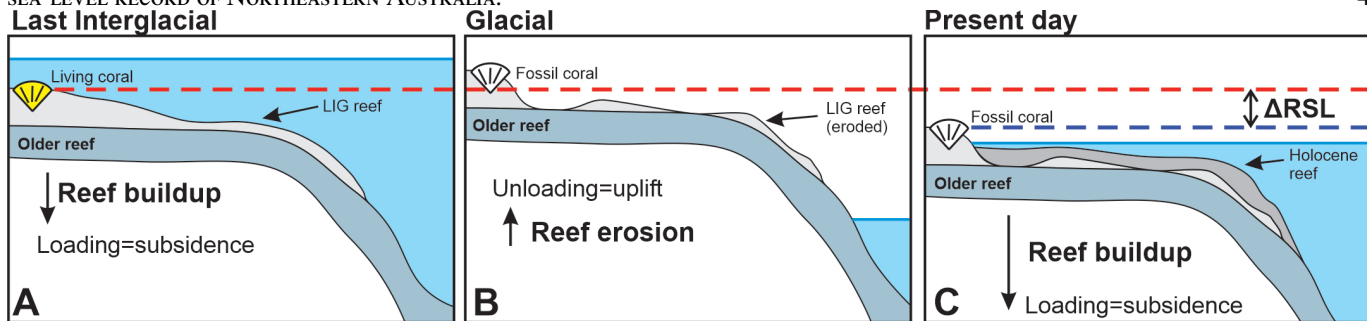


Figure 3: Illustration of reef isostasy caused by the buildup of the reef complex since the Last Interglacial. **A.** The LIG reef is built on top of an older reef (or the bedrock). The addition of this load leads to isostatic subsidence of the underlying bedrock. **B.** As GMSL falls (e.g., under glacial conditions), the reef is partially eroded and/or dissolved (e.g., by karst processes), resulting in isostatic rebound. **C.** As sea level rises a second time, the reef starts to build again on top of previous structures, causing additional subsidence. ΔRSL represents the relative sea-level change caused by reef isostasy. The colored dashed lines represent the the elevation of the coral during the LIG (red) and its present-day elevation (violet). Note that the uplift and subsidence following reef loading and unloading are transient through glacial-interglacial times, and that in our study we do not model the uplift following reef erosion, which we consider to be balanced with Holocene re-growth.

156 significant load on the underlying crust. This loading causes an
 157 isostatic response that is non-negligible. Hereafter, we define
 158 the isostatic adjustment induced by coral reef building as “*reef*
 159 *isostasy*”.

160 An illustration of how reef isostasy impacts the elevation of
 161 a LIG reef measured today is shown in Figure 3. During the
 162 LIG, reef builds on top of an older reef surface (or the basement,
 163 Figure 3A). This loading induces isostatic adjustment, causing
 164 subsidence, or equivalently a relative sea-level rise. The sea-
 165 level change ΔRSL magnitude induced by reef isostasy depends
 166 on reef thickness as well as its geographic extent. Areas with
 167 widespread reef coverage (larger in areal extent than the effective
 168 lithospheric thickness) produce a longer wavelength isostatic sig-
 169 nals, and therefore a larger magnitude relative sea-level change
 170 associated with reef isostasy. In contrast, less extensive reef
 171 coverage, smaller in areal extent than the effective lithospheric
 172 thickness of 50–100 km in this region [6], produce a minimal iso-
 173 static response. During a subsequent glacial period of lower sea
 174 level, erosion and karstification may lead to unloading-induced
 175 uplift that partially compensates for the subsidence during reef
 176 building Figure 3B)

177 An increase in local relative sea-level from crustal subsidence
 178 induced by reef isostasy results in lower elevation LIG coral
 179 sea-level markers today, compared to their original elevation at
 180 the LIG. Therefore LIG coral reef sea-level marker elevations
 181 must be corrected upwards to account for reef isostasy, poten-
 182 tially resulting in higher reconstructed LIG GMSL than prior
 183 estimates.

184 3 RESULTS & DISCUSSION

185 3.1 Reef isostasy: high vs coarse resolution

186 Figure 4 (right panels) shows the elevation change a LIG sea
 187 level marker would undergo from 122 ka to 0 ka due to reef
 188 isostasy (negative values signify that sea-level markers experi-
 189 enced subsidence since the LIG). Our high-resolution simulation
 190 of reef isostasy in the Great Barrier Reef predicts a maximum

relative sea level change of 0.34 m since the Last Interglacial
 191 (Figure 4B). These maximum values are reached in Northeast-
 192 ern Queensland and along the coastline of the southern GBR.
 193 Our predictions for relative sea level change due to reef isostasy
 194 suggest this process is negligible compared to other uncertain-
 195 ties on the paleoelevation of LIG coral reefs (for example coral
 196 growth depths, tides etc.). In contrast, the coarse resolution
 197 reef isostasy calculations (using a 1D GIA model set up and a
 198 loading scenario that does not account for reef coverage area)
 199 predict a maximum relative sea level change of 1.45 m since the
 200 Last Interglacial (Figure 4D). The discrepancy between high vs.
 201 coarse resolution models is due to the fact that the high reso-
 202 lution calculation involves a more localized loading geometry
 203 (and thus reduced crustal deflection) due to elastic compensation
 204 within the lithosphere.

Because high-resolution modeling using the 3D sea-level model
 205 is computationally expensive, we also tested whether a 1D sea-
 206 level model could accurately capture the pattern and magnitude
 207 of relative sea level change due to reef isostasy. We used the
 208 high resolution coral reef loading scenario (paired with the 3D
 209 sea-level model) and first multiplied the loading grid by the
 210 fractional area of reef coverage on a 1 km scale. We then inter-
 211 polated this loading scenario onto a grid with ~34 km resolution
 212 to create a coarse grid that accounts for fractional area of reef
 213 coverage (Figure 4E). We ran a 1D sea-level model with this
 214 loading scenario using the same Earth model as in the other 1D
 215 calculation. This simulation resulted in a similar magnitude of
 216 reef isostasy as in the 3D sea-level high-resolution model, with
 217 a maximum value of 0.4 m of RSL change since the LIG (Figure
 218 4F). However, the spatial pattern does not reproduce the signal
 219 along the southern Great Barrier Reef coastline shown in the 3D
 220 sea-level high resolution simulations. This difference is likely
 221 due to the higher resolution associated with the 3D sea-level
 222 simulation rather than 3D earth structure, as the coarse resolu-
 223 tion 1D calculation does not capture the reef loading regions
 224 along the central and southern Great Barrier Reef coastline.

To assess the sensitivity of our results to Earth structure pa-
 225 rameters, we also performed 1D sea-level simulations using an

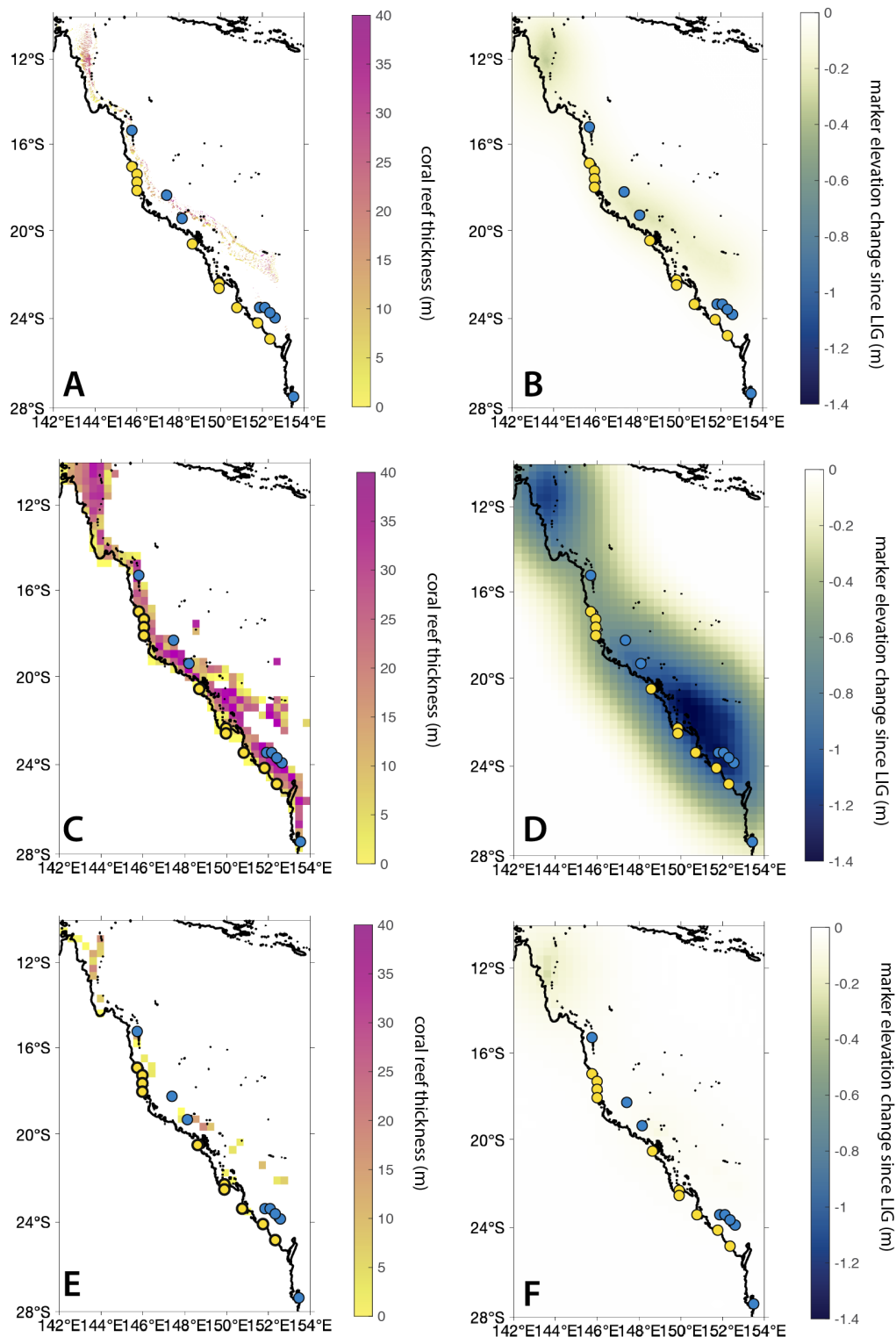


Figure 4: **A.** High resolution coral reef thickness (122-0 ka) for the reef isostasy loading scenario. **B.** Predicted marker elevation change since LIG due to reef isostasy in response to loading in frame A. **C-D.** As in A-B, except for the coarse resolution modeling. **E-F.** As in C-D, except for the coarse resolution treatment of reef thickness (122-0 ka) accounting for reef area coverage. Yellow and blue dots in each map represent the sites shown in Figure 1

229 alternate Earth model, VM2 [63]. We found that changing the
230 Earth model had a negligible effect, perturbing the predicted RSL
231 change by a maximum of 3% at the Queensland/GBR sea-level
232 indicator sites.

233 3.2 Contribution of other geodynamic processes

234 We predicted the elevation change due to reef isostasy (Figure
235 5A), dynamic topography (Figure 5B), and glacial isostatic ad-
236 justment (Figure 5C) from 127 ka to present day. These values
237 represent the elevation change a LIG sea-level indicator would
238 undergo from 127 ka to 0 ka (negative values signify that sea-
239 level indicators experienced subsidence, positive values signify
240 that sea-level indicators experienced uplift since the LIG). The
241 total predicted influence on Last Interglacial sea-level indicator
242 elevation from these geodynamic processes is shown in Figure
243 5D.

244 Our dynamic topography predictions show an elevation change
245 of -10 to 10 m from 127 ka to present day. This means that dy-
246 namic topography would have uplifted the Australian continent
247 by up to 10 m, while offshore regions on the continental shelf
248 would have subsided up to 5 to 10 m since the LIG. Variations in
249 input density and viscosity structure lead to $\sim \pm 1$ m uncertainty
250 in post-LIG dynamic topography change (based on standard
251 deviation of 15 model predictions), and the spatial pattern is
252 remarkably consistent amongst the 15 models investigated here.
253 These results suggest that our predictions of convectively driven
254 onshore-offshore tilting are robust. This inference is corrobo-
255 rated by ~ 100 m Myr $^{-1}$ uplift rates inferred from river profile
256 modelling [17] and patterns of Late Cenozoic age-independent
257 magmatism [7], both features that have been attributed to the
258 presence of an active small-scale convection cell beneath the
259 Queensland margin. Although the dynamic topography maxima
260 and minima are offset with respect to the observed relative sea
261 level maxima and minima, the highest horizontal resolution for
262 the dynamic topography predictions is ~ 200 km, and therefore
263 it may not be possible to precisely match the observed tilting at
264 this resolution.

265 Similarly, glacial isostatic adjustment would have produced
266 uplift on the continent and subsidence offshore. Our predictions
267 show that the continent may have uplifted 6 m and offshore
268 regions subsided 2 m since the Last Interglacial. The spatial
269 variability in elevation change due to glacial isostatic adjustment
270 is caused by the process known as continental levering, where
271 uplift occurs along continental margins as sea-level rise causes
272 subsidence in ocean basins due to additional loading [57].

273 In this study, we did not model some other potential mechanisms
274 that may cause departure from eustasy in the study area. For
275 example, crustal deformation due to re-activation of older faults
276 has been inferred to affect Holocene reefs [see 73, and references
277 therein]. While such mechanism might have relevant local effect,
278 any fault system causing crustal motions would have to be active
279 (with roughly the same deformation rates) over nearly 2000 km
280 of coast to reconcile the observed onshore-offshore tilting trend.
281 This seems an unlikely pattern in an intraplate margin setting
282 such as the Queensland-GBR area. Another process we did not
283 model is the isostatic response to siliciclastic sediment loading.
284 While this process may be relevant at some locations (e.g., on
285 the shelf in front of large rivers, with relevant sediment inputs on
286 the shelf), studies on the Central GBR shelf suggested that the

287 thickness of Holocene sediments is rather limited [<2.5 m 44],
288 hence siliciclastic sediment isostasy is unlikely to explain the
289 difference between onshore and offshore LIG sea-level proxies,
290 recorded over such a large latitudinal gradient.

291 4 CONCLUSIONS

292 The Queensland - GBR area is characterized by an enigmatic
293 difference in the elevation of LIG sea-level indicators between
294 offshore (GBR) and onshore (Queensland coast) sites. This
295 offset motivated our study's modeling of local post-depositional
296 vertical land motion. We modelled sea-level change due to reef
297 isostasy, dynamic topography, and glacial isostatic adjustment
298 since the LIG in this area, which is located on a passive margin
299 spanning a latitudinal range of almost 2000 km. Our models
300 explored whether reef isostasy, which is considered here for
301 the first time, may play a role in the vertical displacement of
302 LIG fossil reefs, which are among the most frequently used
303 geological sea-level proxies [82, 21, 62].

304 In our study area, the contribution of reef isostasy to vertical
305 land motions is negligible, reaching maximum values of 0.34m.
306 In terms of GMSL, this is roughly equivalent to half the contribu-
307 tion of mountain glaciers melting and thermal expansion during
308 the LIG (estimated as up to 1m; 22). Reef isostasy therefore
309 produces a small change in RSL since the LIG at the GBR, and
310 is insufficient in magnitude to explain discrepancies between
311 observed LIG RSL markers offshore and onshore. However,
312 we highlight that this mechanism may represent a potentially
313 important contribution to vertical land motions in areas with
314 dense and widespread coral reef coverage. Therefore, it should
315 be always considered as a potential bias towards higher GMSL
316 in areas with widespread reef coverage.

317 To realistically represent coral reef loading since the LIG in
318 a given area, it is important to gather direct measurements of
319 reef thickness, extent, density and porosity, together with esti-
320 mates of mass loss since the LIG (e.g., due to erosion or karst
321 processes, which we do not model here) and, in the case of
322 wide lagoons, carbonate sediment production from the reef. Our
323 results also underscore the importance of high resolution mod-
324 eling, especially in accounting for the areal coverage of coral
325 reefs, to accurately reproduce relative sea level change due to
326 reef isostasy. Although 1D sea-level models are more computa-
327 tionally efficient, for small-scale loading patterns such as coral
328 reefs, it may be important to use grid refinement in 3D modeling
329 (or high resolution, accounting for reef coverage) in order to
330 accurately capture relative sea level response to reef loading.

331 Comparing the modeled relative contributions of reef isostasy,
332 dynamic topography, and glacial isostatic adjustment, we sur-
333 mise that only the predicted changes due to dynamic topography
334 across sites has a similar magnitude to the differences in sea-
335 level indicators elevation between onshore and offshore. Our
336 dynamic topography simulations, in contrast to reef isostasy
337 and GIA modeling, predict trends of uplift on the continent and
338 subsidence offshore of a magnitude similar to the observed in
339 relative sea-level proxies. This result strengthens the idea that
340 dynamic topography may play a major role in the vertical dis-
341 placement of LIG sea-level indicators [5]. Therefore we suggest
342 that, along the GBR, dynamic topography driven by mantle
343 convection movements may capture the majority of the "long-term"

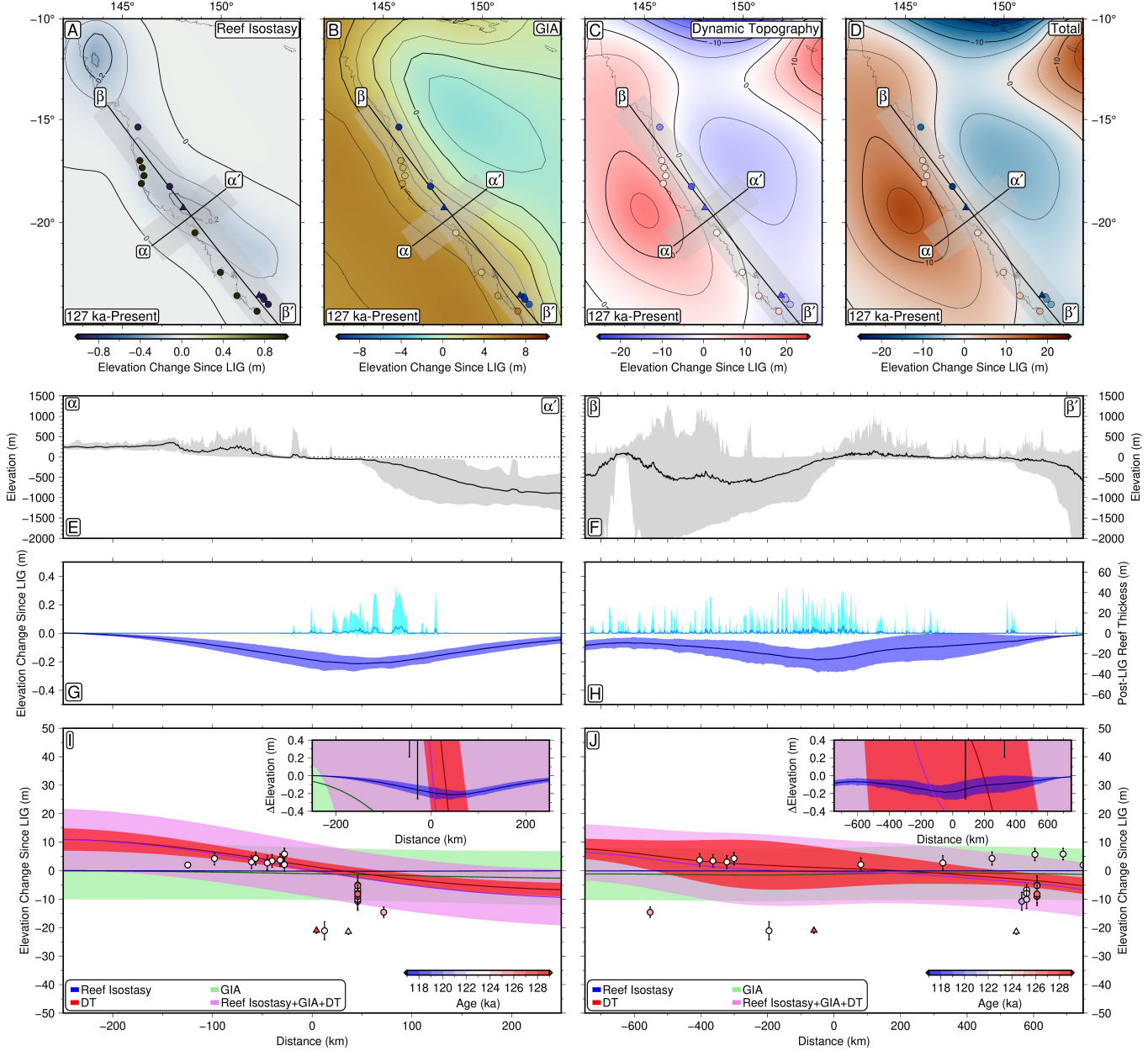


Figure 5: A-C. Predicted elevation change to sea-level indicators from 127 to 0 ka due to: A. reef isostasy B. dynamic topography C. glacial isostatic adjustment. Colored circles represent LIG sea-level indicators as shown in Figure 1. D. Total predicted elevation change to sea-level indicators from 127 to 0 ka. E-F. Gray represents observed elevation range and black line represents mean values for transect $\alpha-\alpha'$ (left) and $\beta-\beta'$ (right). G-H. Light blue line and envelope represents the observed range in reef thicknesses in coral reef loading scenario from LIG to present. Dark blue line and envelope represents the predicted elevation change to sea-level markers due to reef isostasy (as in Figure 5A). Lines represent mean values based on spatial uncertainty of 100 km on either side of transect and intermodel variation uncertainty; envelopes represent the 2 sigma combined uncertainty. I-J. GBR LIG sea-level data points projected onto transects $\alpha-\alpha'$ (left) and $\beta-\beta'$ (right) as a function of distance between the data point and the closest point on the transect. Colored circles/triangles represent LIG sea-level indicator ages. Predicted elevation change projected onto transect A (left) and B (right) for reef isostasy (blue), dynamic topography (red), glacial isostatic adjustment (green), and total (pink). Lines and envelope calculated as in G-H

344 subsidence that was noted by previous studies [53] attempting to
 345 explain the conundrum of lower-than-present LIG reefs on the
 346 Great Barrier Reef. This is thus an important avenue for future
 347 work as improved models of mantle heterogeneity beneath the
 348 area become available.

349 5 METHODS

350 5.0.1 Constructing the coral reef loading scenario

351 As a baseline dataset for the presence/absence of coral reefs, we
 352 used the 500×500 m raster dataset [11, 12, 42] of the warm-water
 353 reefs map compiled by UNEP-WCMC, WorldFish Centre, WRI,
 354 TNC [83, 40, 41, 79]. We created a coral reef loading scenario
 355 since the Last Interglacial (122-0 ka) using two methods, with
 356 different resolutions. For the "coarse resolution grid", we used
 357 standard approach for sea-level model calculations and placed
 358 our coral loading scenario onto a ~ 34 km resolution grid. For
 359 the "high resolution grid", we placed our coral loading scenario
 360 onto a 1 km resolution grid, and accounted for the areal fraction
 361 of coral reef coverage within each 1 km \times 1 km grid cell.

362 Because the GBR reef is characterized by narrow, sometimes
 363 isolated, strips of coral reef, we were concerned that the stan-
 364 dard grid resolution (~ 34 km) used in sea-level models may
 365 unrealistically smooth out the reef loading signal. Thus, for the
 366 "high resolution grid" we interpolated a high-resolution Digital
 367 Elevation Model for bathymetry in the Great Barrier Reef area
 368 onto a 1 km resolution grid [8]. We then assessed the fractional
 369 area of reef coverage within each 1 km \times 1 km grid cell using
 370 the "Fishnet" tool of ArcGIS. Of grid cells with non-zero reef
 371 coverage, 44% had full reef coverage (Figure 6). We then multi-
 372 plied the coral reef thickness in our 1 km \times 1 km grids by the
 373 areal fraction of reef coverage to produce our "high resolution
 374 grid" coral reef loading scenario.

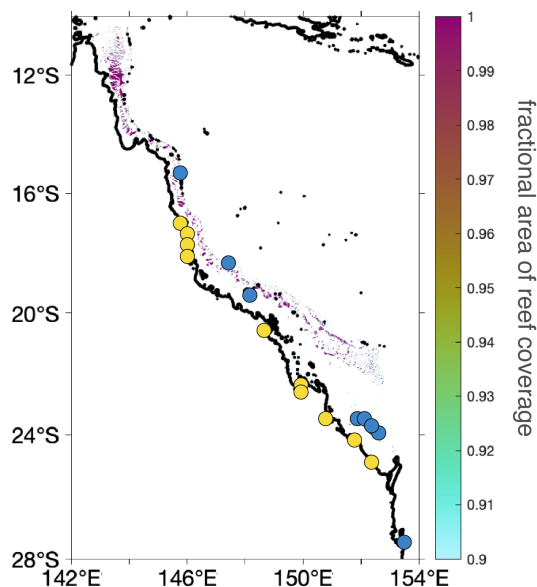


Figure 6: Fractional area of present-day reef coverage. Yellow and blue dots represent the sites shown in Figure 1.

375 We also used a standard approach for constructing a loading
 376 scenario by interpolating a high-resolution bathymetric Digital

Elevation Model of the GBR area onto a Gauss Legendre grid
 377 with ~ 34 km resolution (maximum spherical harmonic degree
 378 512) commonly used in sea-level calculations. This approach
 379 does not account for coral reef coverage since the coral reef
 380 thickness is smoothed over a wide area relative to the lateral
 381 extent of coral reefs. We term this coral reef loading scenario
 382 the "coarse resolution grid" (Figure 4C).

In both scenarios, we assumed that regions with any reef coverage (fractional area of reef coverage > 0 ; Figure 6A) had coral reefs that had grown since the Last Interglacial. We assigned the total coral reef thickness deposited since the Last Interglacial as the modern basement depth (as in, we assumed the coral reef surface grew to modern sea level) in regions with basement depths shallower than 55 m. Below this bathymetry, we considered that no reef was present in the LIG. To partition coral reef loading across 122 to 0 ka, we made the assumption that the Last Interglacial reef thickness would represent 1.5 times the thickness of Holocene coral reef growth, given the longer time available for LIG reefs to grow with respect to Holocene ones. In our models, we assumed a reef porosity of 40% (that is, the porosity of reefs in sand flats/lagoons in the GBR reported by 38) and a coral reef density of 1600 kg/m^3 (equivalent to the average coral colony density as reported by 10 in 38).

For the "high resolution grid" coral loading scenario, we multiplied our map of reef thickness by the fractional area of reef coverage (Figure 6A). This assumes that the coverage hasn't changed since 120 ka. To isolate the impact of reef loading, we did not include ice sheet loading changes in our modeling. Our reef loading scenario introduced the LIG coral thickness at 120 ka and the Holocene coral thickness at 8 ka. Although coral reefs built over a longer time span, we simplified our calculation by introducing the load at a single timestep, assuming that the timing of the load will have a negligible impact at present-day after several thousand years of isostatic adjustment. To conserve mass, we uniformly removed a layer of sediment from the continents with a mass equivalent to the total reef load globally.

Although reef loading prior to the LIG would have induced an ongoing isostatic response at the LIG, our analysis is limited to estimating sea-level change since the LIG due to reef loading over only the last glacial cycle. Thus, we limited our modeling to the period from 122 to 0 ka to assess the magnitude of sea level change due to reef loading since 122 ka.

5.0.2 Modeling Isostatic Adjustment: Reef isostasy

1D calculation (coarse resolution). To calculate relative sea-level change (ΔRSL) in response to reef loading over the last ice age, we used a gravitationally self-consistent sea-level model. We used the coarse resolution coral reef loading scenario as input to a 1D sea-level model, which assumes radially symmetric Earth structure. Our calculations are based on the theory and pseudo-spectral algorithm described by Kendall et al. [46] with a spherical harmonic truncation at degree and order 512 (spatial resolution of ~ 34 km). These calculations include the impact of load-induced Earth rotation changes on sea level [55, 59], evolving shorelines and the migration of grounded, marine-based ice [45, 56, 50, 46]. Our predictions require models for Earth's viscoelastic structure. We adopted an earth model characterized by a lithospheric thickness of 96 km, and upper and lower mantle viscosities of 5×10^{20} and 5×10^{21} Pa s, respectively.

435 **3D calculation (high resolution).** The predicted magnitude of
436 relative sea level change is sensitive to the spatial scale of the
437 load, in addition to the load thickness. To assess whether the
438 coarser resolution accurately captures the crustal deformation
439 (and thus relative sea level) response to reef loading, we next
440 performed calculations using a 3D sea-level model, and the
441 "high resolution grid" coral reef loading scenario with a regional
442 spatial resolution of 1 km that accounts for the fractional area of
443 reef coverage in each grid cell.

444 To solve for relative sea level change in response to coral reef
445 loading on a higher resolution of 1 km, we used a global 3D
446 finite volume sea level and Earth deformation model [51]. The
447 numerical approach incorporates lateral variations in Earth struc-
448 ture and calculates the resulting gravitationally self-consistent
449 sea level change [58]. Previous studies have adopted this com-
450 putational model in order to account for 3D earth structure (e.g.,
451 4, 32, 49). The 3D glacial isostatic adjustment model is capable
452 of km-scale resolution, which is achieved through regional grid
453 refinement for computational efficiency [32]. The importance
454 of high resolution GIA modeling has been demonstrated for
455 the solid Earth response to marine grounding line migration in
456 Antarctica [87]. Grid refinement is achieved by incrementally
457 bisecting grid edges in the selected region to achieve the desired
458 1 km x 1 km resolution, and a final smoothing operation along
459 the region boundary to ensure a well-behaved transition.

460 Our simulation uses a 3D viscoelastic earth model. Here, we
461 apply the hybrid model described in Austermann et al. [6], which
462 infers mantle viscosity from seismic tomography using anelastic
463 scaling relationships and additional information on the thermal
464 and rheological state of the upper mantle. In the upper 400 km,
465 a calibrated parameterisation of anelastic behaviour at seismic
466 frequencies is used to self-consistently determine lithospheric
467 thickness (assumed here to be equivalent to 1175°C isotherm
468 depth) and viscosity variations from the shear-wave velocity (V_S)
469 structure of the tomographic model, SL2013sv [66, 75]. Below
470 400km, viscosities are derived from the shear wave tomography
471 model SEMUCB-WM1 [29]. Austermann et al. (2021) provides
472 details on the V_S to viscosity conversion.

473 In our 3D GIA calculations, viscosity variations are shifted at
474 each depth to average to 5×10^{20} Pa s in the upper mantle vis-
475 cosity 5×10^{21} Pa s in the lower mantle viscosity [65], identical
476 to the earth model used in the 1D GIA calculations. The effec-
477 tive lithospheric thickness in this region varies from 50–100
478 km (Figure SX). We paired this model with the high resolution
479 coral reef loading scenario (Figure 4A) which accounts for reef
480 coverage area at 1 km resolution (Figure 6A).

481 5.1 Modeling Glacial Isostatic Adjustment: Ice loading

482 We modeled relative sea level change in response to ice sheet
483 and ocean loading changes since the LIG using the 1D pseudo-
484 spectral approach described in Kendall et al. [46]. We used
485 the same model and earth structure described in the 1D reef
486 loading sea-level calculations (an Earth model characterized by a
487 lithospheric thickness of 96 km, and p55 upper and lower mantle
488 viscosities (5×10^{20} Pa s and 5×10^{21} Pa s, respectively)).

489 We used an ice history characterized by the GMSL history in
490 Waelbroeck et al. [85] over the last glacial cycle. The ice history
491 was constructed using the ICE-6G deglacial ice geometry history

492 and has no excess melt across the LIG (as in 6). The GMSL
493 history was adjusted at the LIG since the Waelbroeck GMSL
494 history assumes a value of -75 m at 128 ka, which is at odds with
495 coral evidence from the many locations that indicate sea level
496 must have been close to present at that time. To account for this
497 discrepancy, the timing of the GMSL curve is shifted prior to the
498 LIG back by 3.5 ka. This shift allows for a longer interglacial
499 time period without changing the deglaciation pattern of the
500 original curve and places the MIS 6 sea-level low stand at 135.5
501 ka (as in 24).

5.2 Dynamic Topography

502 Observational estimates indicate that mantle flow-driven ver-
503 tical motions can reach rates of $\sim 0.1\text{--}1$ m kyr^{-1} in certain lo-
504 cations, suggesting a significant fraction of relative sea-level
505 change along the Great Barrier Reef from the LIG to present
506 day could result from evolving mantle dynamic topography
507 [36, 86, 5, 81]. To investigate this possibility, we simulate rates
508 of global dynamic topography change using the mantle convection
509 code ASPECT and an ensemble of Earth models based on
510 5 seismic tomographic inversions of deep Earth structure (LLNL-
511 G3D-JPS, 77; S40RTS, 68; SAVANI, 3; SEMUCB-WM1, 29;
512 TX2011, 34) and 3 radial viscosity profiles (S10, 80; F10V1,
513 28; F10V2, 28).

515 Above 300 km, input temperature and density fields are derived
516 from a modified version of the RHGW20 model of Richards
517 et al. [66], which accounts for anelasticity at seismic frequencies
518 and has been demonstrated to yield acceptable fits to present-
519 day short-wavelength dynamic topography. Unlike RHGW20,
520 which is based exclusively on the SL2013sv global surface wave
521 tomographic model [75], the upper mantle model we adopt here
522 is augmented with regional high-resolution tomographic studies
523 in North America (SL2013NA; 74), Africa (AF2019; 14), and
524 South America and the South Atlantic Ocean (SA2019; 13; see
525 37 and 67 for further details). Below 400 km, a thermodynamic
526 modelling approach is used to obtain thermochemical buoyancy
527 structures for each combination of seismic tomographic and
528 rheological input that are compatible with present-day geophysical
529 observables, including geoid anomalies, dynamic topogra-
530 phy, and CMB excess ellipticity, and comprise thermochemical
531 anomalies within the base of LLVPs (67; see Supplementary
532 Material for further details). Between 300 and 400 km, tem-
533 peratures and densities derived from these two independent
534 parameterisations are smoothly merged by taking their weighted
535 average as a function of depth.

536 The time-dependent geodynamic simulations derived from these
537 Earth models assume free-slip conditions at the surface and core-
538 mantle boundary, account for lithospheric cooling by including
539 shallow mantle buoyancy variations and representative thermal
540 conductivity, and incorporate temperature- and composition-
541 dependent viscosity variations (see Supplementary Material for
542 further details). Following [5], we run our models forward in
543 time and, to avoid the potential for transient numerical artefacts
544 in early time steps to affect our results, we assume the average
545 rate of dynamic topography change between 0.5 and 1.5 Ma
546 is representative of that experienced between the LIG and the
547 present day. Change in dynamic topography at specific sea-
548 level sites is calculated by combining perturbations due to the
549 evolving mantle flow pattern with those caused by rigid plate

550 motion across the convective planform. This is accomplished by
551 translating the dynamic topography field calculated for the LIG
552 into its present-day coordinates using plate velocities taken from
553 MORVEL [2], before calculating the difference between this
554 rotated LIG field and the predicted present-day field, yielding
555 a total of 15 individual model predictions. Note that the maxi-
556 mum horizontal resolution of the tomographically derived Earth
557 models is ~200 km, placing an important limit on the minimum
558 wavelength of predicted dynamic topography variations.

559 6 DATA AVAILABILITY

560 Supplementary figures and the datasets used in this study are
561 available open-access as Rovere et al. [70].

562 7 AUTHOR CONTRIBUTIONS

563 The manuscript was written jointly by A.R. and T.P. The initial
564 concept of this work was developed by A.R., M.J.O, I.D.G. and
565 J.X.M. Models of reef isostasy were developed by T.P. Models
566 of dynamic topography and glacial isostatic adjustment were
567 developed by F.R., J.A. and K.L. The parts of the manuscript
568 related to field observations was written by A.R., M.J.O. and
569 I.D.G. The parts of the manuscript related to modelled vertical
570 land motions were written by T.P. and F.R. with inputs from
571 J.X.M., J.A. and K.L.

572 8 ACKNOWLEDGMENTS

573 This work was funded by the European Research Council (ERC)
574 under the European Union’s Horizon 2020 research and inno-
575 vation programme (grant agreement n. 802414 to A.R.). T.P.
576 acknowledges funding from the NSF EAR Postdoctoral Fellow-
577 ship, the University of California President’s Postdoctoral Fel-
578 lowship, and NSF OCE – 2054757. F.D.R. acknowledges fund-
579 ing from the Imperial College Research Fellowship Scheme. J.A.
580 acknowledges funding from NSF grant OCE-1841888. Fund-
581 ing is also acknowledged from Harvard University (J.X.M. and
582 K.L.)

583 REFERENCES

- 584 [1] P. N. Adams, N. D. Opdyke, and J. M. Jaeger. Isostatic up-
585 lift driven by karstification and sea-level oscillation: Mod-
586 eling landscape evolution in north florida. *Geology*, 38(6):
587 531–534, 2010.
- 588 [2] D. F. Argus, R. G. Gordon, and C. DeMets. Geologically
589 current motion of 56 plates relative to the no-net-rotation
590 reference frame. *Geochemistry, Geophysics, Geosystems*,
591 12(11), 2011.
- 592 [3] L. Auer, L. Boschi, T. Becker, T. Nissen-Meyer, and D. Gi-
593 ardini. Savani: A variable resolution whole-mantle model
594 of anisotropic shear velocity variations based on multiple
595 data sets. *Journal of Geophysical Research: Solid Earth*,
596 119(4):3006–3034, 2014.
- 597 [4] J. Austermann, J. X. Mitrovica, K. Latychev, and G. A.
598 Milne. Barbados-based estimate of ice volume at last
599 glacial maximum affected by subducted plate. *Nature
600 Geoscience*, 6(7):553–557, 2013.
- [5] J. Austermann, J. X. Mitrovica, P. Huybers, and A. Ro-
601 vere. Detection of a dynamic topography signal in last
602 interglacial sea-level records. *Science Advances*, 3(7):
603 e1700457, 2017.
- [6] J. Austermann, M. J. Hoggard, K. Latychev, F. D. Richards,
605 and J. X. Mitrovica. The effect of lateral variations in earth
606 structure on last interglacial sea level. *Geophysical Journal
607 International*, 227(3):1938–1960, 2021.
- [7] P. Ball, K. Czarnota, N. White, M. Klöcking, and D. Davies.
609 Thermal structure of eastern australia’s upper mantle and
610 its relationship to cenozoic volcanic activity and dynamic
611 topography. *Geochemistry, Geophysics, Geosystems*, 22
612 (8):e2021GC009717, 2021.
- [8] R. Beaman. High-resolution depth model for the great
614 barrier reef and coral sea - 100 m, 2020.
- [9] B. P. Brooke, Z. Huang, W. A. Nicholas, T. S. Oliver,
616 T. Tamura, C. D. Woodroffe, and S. L. Nichol. Rela-
617 tive sea-level records preserved in holocene beach-ridge
618 strandplains—an example from tropical northeastern aus-
619 tralia. *Marine Geology*, 411:107–118, 2019.
- [10] R. W. Buddemeier, J. E. Maragos, and D. W. Knutson.
621 Radiographic studies of reef coral exoskeletons: rates and
622 patterns of coral growth. *Journal of Experimental Marine
623 Biology and Ecology*, 14(2):179–199, 1974.
- [11] L. Burke, K. Reytar, M. Spalding, and A. Perry. Reefs at
625 risk revisited: technical notes on modeling threats to the
626 world’s coral reefs. *Washington, DC: World Resources
627 Institute*, 2011.
- [12] L. Burke, K. Reytar, M. Spalding, and A. Perry. *Reefs at
629 risk revisited*. World Resources Institute, 2011.
- [13] N. L. Celli, S. Lebedev, A. J. Schaeffer, and C. Gaina.
631 African cratonic lithosphere carved by mantle plumes. *Nature
632 Communications*, 11(92):1–10, 2020. ISSN 20411723.
633 doi: 10.1038/s41467-019-13871-2.
- [14] N. L. Celli, S. Lebedev, A. J. Schaeffer, M. Ravenna, and
635 C. Gaina. The upper mantle beneath the South Atlantic
636 Ocean, South America and Africa from waveform tomo-
637 graphy with massive data sets. *Geophysical Journal In-
638 ternational*, 221:178–204, 2020. ISSN 0956-540X. doi:
639 10.1093/gji/ggz574.
- [15] P. M. Chutcharavan and A. Dutton. A global com-
641 pilation of u-series-dated fossil coral sea-level indica-
642 tors for the last interglacial period (marine isotope stage
643 5e). *Earth System Science Data*, 13(7):3155–3178, 2021.
644 doi: 10.5194/essd-13-3155-2021. URL <https://essd.copernicus.org/articles/13/3155/2021/>.
- [16] J. R. Creveling, J. Austermann, and A. Dutton. Uplift of
647 trail ridge, florida, by karst dissolution, glacial isostatic ad-
648 justment, and dynamic topography. *Journal of Geophysical
649 Research: Solid Earth*, 2019.
- [17] K. Czarnota, G. Roberts, N. White, and S. Fishwick. Spa-
651 tial and temporal patterns of australian dynamic topo-
652 graphy from river profile modeling. *Journal of Geophysical
653 Research: Solid Earth*, 119(2):1384–1424, 2014.
- [18] A. Dalca, K. Ferrier, J. X. Mitrovica, J. Perron, G. Milne,
655 and J. Creveling. On postglacial sea level—iii. incorporat-

- 657 ing sediment redistribution. *Geophysical Journal International*, 194(1):45–60, 2013.

658

659 [19] B. Dechnik, J. M. Webster, G. E. Webb, L. Nothdurft,
660 A. Dutton, J. C. Braga, J.-x. Zhao, S. Duce, and J. Sadler.
661 The evolution of the great barrier reef during the last inter-
662 glacial period. *Global and Planetary Change*, 149:53–71,
663 2017.

664 [20] B. Dechnik, J. M. Webster, G. E. Webb, L. Noth-
665 durft, and J.-x. Zhao. Successive phases of holocene
666 reef flat development: Evidence from the mid- to
667 outer great barrier reef. *Palaeogeography, Palaeocli-
668 matology, Palaeoecology*, 466:221–230, 2017. ISSN
669 0031-0182. doi: <https://doi.org/10.1016/j.palaeo.2016.11.030>. URL <https://www.sciencedirect.com/science/article/pii/S0031018216304412>.

670 [21] A. Dutton and K. Lambeck. Ice volume and sea level
671 during the last interglacial. *science*, 337(6091):216–219,
672 2012.

673 [22] A. Dutton, A. E. Carlson, A. J. Long, G. A. Milne, P. U.
674 Clark, R. DeConto, B. P. Horton, S. Rahmstorf, and M. E.
675 Raymo. Sea-level rise due to polar ice-sheet mass loss
676 during past warm periods. *science*, 349(6244):aaa4019,
677 2015.

678 [23] A. Dutton, J. M. Webster, D. Zwart, K. Lambeck, and
679 B. Wohlfarth. Tropical tales of polar ice: evidence of last
680 interglacial polar ice sheet retreat recorded by fossil reefs
681 of the granitic seychelles islands. *Quaternary Science
682 Reviews*, 107:182–196, 2015.

683 [24] B. Dyer, J. Austermann, W. J. D’Andrea, R. C. Creel, M. R.
684 Sandstrom, M. Cashman, A. Rovere, and M. E. Raymo.
685 Sea-level trends across the Bahamas constrain peak last
686 interglacial ice melt. *Proceedings of the National Academy
687 of Sciences of the United States of America*, 118(33):1–11,
688 2021. ISSN 10916490. doi: 10.1073/pnas.2026839118.

689 [25] W. Farrell and J. A. Clark. On postglacial sea level. *Geo-
690 physical Journal International*, 46(3):647–667, 1976.

691 [26] K. L. Ferrier, J. X. Mitrovica, L. Giosan, and P. D. Clift.
692 Sea-level responses to erosion and deposition of sediment
693 in the indus river basin and the arabian sea. *Earth and
694 Planetary Science Letters*, 416:12–20, 2015.

695 [27] K. L. Ferrier, J. Austermann, J. X. Mitrovica, and T. Pico.
696 Incorporating sediment compaction into a gravitationally
697 self-consistent model for ice age sea-level change. *Geo-
698 physical Journal International*, 211(1):663–672, 2017.

699 [28] A. M. Forte, S. Quéré, R. Moucha, N. A. Simmons, S. P.
700 Grand, J. X. Mitrovica, and D. B. Rowley. Joint seismic-
701 geodynamic-mineral physical modelling of African geody-
702 namics: A reconciliation of deep-mantle convection with
703 surface geophysical constraints. *Earth and Planetary Sci-
704 ence Letters*, 295(3-4):329–341, 2010.

705 [29] S. W. French and B. Romanowicz. Broad plumes rooted
706 at the base of the Earth’s mantle beneath major hotspots.
707 *Nature*, 525(7567):95–99, 2015. ISSN 0028-0836. doi:
708 10.1038/nature14876.

709 [30] M. K. Gagan, D. P. Johnson, and G. M. Crowley. Sea
710 level control of stacked late quaternary coastal sequences,
711 central great barrier reef. *Sedimentology*, 41(2):329–351,
712 1994.

713 [31] Geoscience Australia. *Digital Elevation Model (DEM)
714 of Australia derived from LiDAR 5 Metre Grid*. Aus-
715 tralian Government, Canberra, 2015. doi: <https://doi.org/10.26186/89644>.

716 [32] N. Gomez, K. Latychev, and D. Pollard. A coupled ice
717 sheet–sea level model incorporating 3d earth structure:
718 Variations in antarctica during the last deglacial retreat.
719 *Journal of Climate*, 31(10):4041–4054, 2018.

720 [33] I. D. Goodwin. Last interglacial sea-level and wave climate
721 change in the subtropical south-west pacific. in prep.

722 [34] S. P. Grand. Mantle shear-wave tomography and the fate of
723 subducted slabs. *Philosophical Transactions of the Royal
724 Society of London. Series A: Mathematical, Physical and
725 Engineering Sciences*, 360(1800):2475–2491, 2002.

726 [35] J. M. Gregory, S. M. Griffies, C. W. Hughes, J. A. Lowe,
727 J. A. Church, I. Fukimori, N. Gomez, R. E. Kopp, F. Lan-
728 derer, G. L. Cozannet, R. Ponte, D. Stammer, M. E.
729 Tamisiea, and R. S. W. van de Wal. Concepts and ter-
730 minology for sea level: Mean, variability and change, both
731 local and global. *Surveys in Geophysics*, 40(6):1251–1289,
732 2019.

733 [36] R. A. Hartley, G. G. Roberts, N. White, and C. Richardson.
734 Transient convective uplift of an ancient buried landscape.
735 *Nature Geoscience*, 4(8):562–565, 2011.

736 [37] M. J. Hoggard, K. Czarnota, F. D. Richards, D. L. Huston,
737 A. L. Jaques, and S. Ghelichkhan. Global distribution of
738 sediment-hosted metals controlled by craton edge stability.
739 *Nature Geoscience*, 13:504–510, 2020.

740 [38] D. Hopley. *Density and PorosityDensity and Porosity: In-
741 fluence on Reef Accretion Rates*, pages 303–304. Springer
742 Netherlands, Dordrecht, 2011. ISBN 978-90-481-2639-
743 2. doi: 10.1007/978-90-481-2639-2_275. URL https://doi.org/10.1007/978-90-481-2639-2_275.

744 [39] D. Hopley, S. G. Smithers, and K. Parnell. *The geomor-
745 phology of the Great Barrier Reef: development, diversity
746 and change*. Cambridge University Press, 2007.

747 [40] IMaRS-USF. Millennium coral reef mapping project. un-
748 validated maps, 2005.

749 [41] IMaRS-USF, IRD. Millennium coral reef mapping project.
750 validated maps, 2005.

751 [42] Institute for Marine Remote Sensing, University of South
752 Florida (IMaRS/USF) Institut de Recherche pour le
753 Développement (IRD), UNEP-WCMC, The WorldFish
754 Center, and WRI,. Global Coral Reefs composite dataset
755 compiled from multiple sources for use in the Reefs at Risk
756 Revisited project incorporating products from the Millen-
757 nium Coral Reef Mapping Project prepared by IMaRS/USF
758 and IRD, 2011.

759 [43] IPCC. Ipcc special report on the ocean and cryosphere in
760 a changing climate. 2019.

761 [44] D. Johnson and D. Searle. Post-glacial seismic stratigraphy,
762 central great barrier reef, australia. *Sedimentology*, 31(3):
763 335–352, 1984.

764 [45] P. Johnston. The effect of spatially non-uniform water loads
765 on prediction of sea-level change. *Geophysical Journal
766 International*, 114(3):615–634, 1993.

- [46] R. A. Kendall, J. X. Mitrovica, and G. A. Milne. On post-glacial sea level–ii. numerical formulation and comparative results on spherically symmetric models. *Geophysical Journal International*, 161(3):679–706, 2005.
- [47] J. A. Kleypas. *Geological development of fringing reefs in the Southern Great Barrier Reef, Australia*. James Cook University of North Queensland, 1991.
- [48] J. A. Kleypas and D. Hopley. Reef development across a broad continental shelf, southern great barrier reef, australia. In *Proc*, volume 7, pages 1129–1141, 1992.
- [49] J. Kuchar, G. Milne, and K. Latychev. The importance of lateral earth structure for north american glacial isostatic adjustment. *Earth and Planetary Science Letters*, 512: 236–245, 2019.
- [50] K. Lambeck, A. Purcell, P. Johnston, M. Nakada, and Y. Yokoyama. Water-load definition in the glacio-hydro-isostatic sea-level equation. *Quaternary Science Reviews*, 22(2-4):309–318, 2003.
- [51] K. Latychev, J. X. Mitrovica, J. Tromp, M. E. Tamisiea, D. Komatsitsch, and C. C. Christara. Glacial isostatic adjustment on 3-d earth models: a finite-volume formulation. *Geophysical Journal International*, 161(2):421–444, 2005.
- [52] T. Lorscheid and A. Rovere. The indicative meaning calculator–quantification of paleo sea-level relationships by using global wave and tide datasets. *Open Geospatial Data, Software and Standards*, 4(1):1–8, 2019.
- [53] J. F. Marshall and P. J. Davies. Last interglacial reef growth beneath modern reefs in the southern great barrier reef. *Nature*, 307(5946):44–46, 1984.
- [54] M. T. McCulloch and T. Esat. The coral record of last interglacial sea levels and sea surface temperatures. *Chemical Geology*, 169(1-2):107–129, 2000.
- [55] G. A. Milne and J. X. Mitrovica. Postglacial sea-level change on a rotating earth: first results from a gravitationally self-consistent sea-level equation. *Geophysical Journal International*, 126(3):F13–F20, 1996.
- [56] G. A. Milne, J. X. Mitrovica, and J. L. Davis. Near-field hydro-isostasy: the implementation of a revised sea-level equation. *Geophysical Journal International*, 139(2):464–482, 1999.
- [57] J. X. Mitrovica and G. Milne. On the origin of late holocene sea-level highstands within equatorial ocean basins. *Quaternary Science Reviews*, 21(20-22):2179–2190, 2002.
- [58] J. X. Mitrovica and G. A. Milne. On post-glacial sea level: I. general theory. *Geophysical Journal International*, 154 (2):253–267, 2003.
- [59] J. X. Mitrovica, J. Wahr, I. Matsuyama, and A. Paulson. The rotational stability of an ice-age earth. *Geophysical Journal International*, 161(2):491–506, 2005.
- [60] C. Murray-Wallace and A. Belperio. The last interglacial shoreline in australia—a review. *Quaternary Science Reviews*, 10(5):441–461, 1991.
- [61] N. Opdyke, D. Spangler, D. Smith, D. Jones, and R. Lindquist. Origin of the epeirogenic uplift of pliocene-pleistocene beach ridges in florida and development of the florida karst. *Geology*, 12(4):226–228, 1984.
- [62] M. J. O’Leary, P. J. Hearty, W. G. Thompson, M. E. Raymo, J. X. Mitrovica, and J. M. Webster. Ice sheet collapse following a prolonged period of stable sea level during the last interglacial. *Nature Geoscience*, 6(9):796–800, 2013.
- [63] W. Peltier and R. G. Fairbanks. Global glacial ice volume and last glacial maximum duration from an extended barbados sea level record. *Quaternary Science Reviews*, 25 (23-24):3322–3337, 2006.
- [64] T. Pico, J. X. Mitrovica, K. L. Ferrier, and J. Braun. Global ice volume during mis 3 inferred from a sea-level analysis of sedimentary core records in the yellow river delta. *Quaternary Science Reviews*, 152:72–79, 2016.
- [65] M. E. Raymo, J. X. Mitrovica, M. J. O’Leary, R. M. DeConto, and P. J. Hearty. Departures from eustasy in pliocene sea-level records. *Nature Geoscience*, 4(5):328–332, 2011.
- [66] F. D. Richards, M. J. Hoggard, N. White, and S. Ghelichkhan. Quantifying the relationship between short-wavelength dynamic topography and thermomechanical structure of the upper mantle using calibrated parameterization of anelasticity. *Journal of Geophysical Research: Solid Earth*, 125:e2019JB019062, 2020. doi: 10.1029/2019JB019062.
- [67] F. D. Richards, M. J. Hoggard, S. Ghelichkhan, P. Koolemeijer, and H. Lau. Geodynamic, geodetic, and seismic constraints favour deflated and dense-cored llvps. *Earth ArXiv*, 2021.
- [68] J. Ritsema, A. Deuss, H. J. Van Heijst, and J. H. Woodhouse. S4ORTS: A degree-40 shear-velocity model for the mantle from new Rayleigh wave dispersion, teleseismic traveltimes and normal-mode splitting function measurements. *Geophysical Journal International*, 184:1223–1236, 2011. ISSN 0956540X. doi: 10.1111/j.1365-246X.2010.04884.x.
- [69] A. Rovere, P. Stocchi, and M. Vacchi. Eustatic and relative sea level changes. *Current Climate Change Reports*, 2(4): 221–231, 2016.
- [70] A. Rovere, T. Pico, F. Richards, M. J. O’Leary, J. X. Mitrovica, I. D. Goodwin, J. Austermann, and K. Latychev. Supplementary data for: "The influence of reef isostasy, dynamic topography, and glacial isostatic adjustment on the Last Interglacial sea- level record of Northeastern Australia", Aug. 2022. URL <https://doi.org/10.5281/zenodo.6957644>.
- [71] G. A. Ruettner, K. L. Ferrier, J. R. Creveling, and M. Fox. Sea-level responses to rapid sediment erosion and deposition in taiwan. *Earth and Planetary Science Letters*, 538: 116198, 2020.
- [72] E. Ryan, S. Smithers, S. Lewis, T. Clark, J.-X. Zhao, and Q. Hua. Fringing reef growth over a shallow last interglacial reef foundation at a mid-shelf high island: Holbourne island, central great barrier reef. *Marine Geology*, 398:137–150, 2018.
- [73] A. Sansoleimani, G. E. Webb, D. L. Harris, S. R. Phinn, and C. M. Roelfsema. Antecedent topography and active tectonic controls on holocene reef geomorphology in the great barrier reef. *Geomorphology*, 413:108354, 2022.

- 885 ISSN 0169-555X. doi: <https://doi.org/10.1016/j.geomorph.2022.108354>. URL <https://www.sciencedirect.com/science/article/pii/S0169555X22002471>.
- 886 [74] A. Schaeffer and S. Lebedev. Imaging the north american continent using waveform inversion of global and usarray data. *Earth and Planetary Science Letters*, 402:26–41, 2014.
- 887 [75] A. J. Schaeffer and S. Lebedev. Global shear speed structure of the upper mantle and transition zone. *Geophysical Journal International*, 194:417–449, 2013. ISSN 0956540X. doi: 10.1093/gji/ggt095.
- 888 [76] I. Shennan, A. J. Long, and B. P. Horton. *Handbook of sea-level research*. John Wiley & Sons, 2015.
- 889 [77] N. Simmons, S. Myers, G. Johannesson, E. Matzel, and S. Grand. Evidence for long-lived subduction of an ancient tectonic plate beneath the southern Indian Ocean. *Geophysical Research Letters*, 42(21):9270–9278, 2015.
- 890 [78] A. Skrivanek, J. Li, and A. Dutton. Relative sea-level change during the last interglacial as recorded in bahamian fossil reefs. *Quaternary Science Reviews*, 200:160 – 177, 2018. ISSN 0277-3791. doi: <https://doi.org/10.1016/j.quascirev.2018.09.033>. URL <http://www.sciencedirect.com/science/article/pii/S0277379118304384>.
- 891 [79] M. Spalding, M. D. Spalding, C. Ravilious, and E. P. Green. *World atlas of coral reefs*. Univ of California Press, 2001.
- 892 [80] B. Steinberger, S. C. Werner, and T. H. Torsvik. Deep versus shallow origin of gravity anomalies, topography and volcanism on Earth, Venus and Mars. *Icarus*, 207(2):564–577, 2010.
- 893 [81] S. N. Stephenson, N. J. White, T. Li, and L. F. Robinson. Disentangling interglacial sea level and global dynamic topography: Analysis of madagascar. *Earth and Planetary Science Letters*, 519:61–69, 2019.
- 894 [82] C. Stirling, T. Esat, K. Lambeck, and M. McCulloch. Timing and duration of the last interglacial: evidence for a restricted interval of widespread coral reef growth. *Earth and Planetary Science Letters*, 160(3-4):745–762, 1998.
- 895 [83] UNEP-WCMC, WorldFish Centre, WRI, TNC. Global distribution of warm-water coral reefs, compiled from multiple sources including the millennium coral reef mapping project. version 4.0, 2010. <http://data.unep-wcmc.org/datasets/1>.
- 896 [84] O. Van de Plassche. Sea-level research: A manual for the collection and evaluation of data: Norwich. UK, Geobooks, 1986.
- 897 [85] C. Waelbroeck, L. Labeyrie, E. Michel, J.-C. Duplessy, J. F. Mcmanus, K. Lambeck, E. Balbon, and M. Labracherie. Sea-level and deep water temperature changes derived from benthic foraminifera isotopic records. *Quaternary science reviews*, 21(1-3):295–305, 2002.
- 898 [86] R. Walker, M. Telfer, R. Kahle, M. Dee, B. Kahle, J.-L. Schwenninger, R. Sloan, and A. Watts. Rapid mantle-driven uplift along the angolan margin in the late quaternary. *Nature Geoscience*, 9(12):909–914, 2016.
- [87] J. X. W. Wan, N. Gomez, K. Latychev, and H. K. Han. Resolving glacial isostatic adjustment (gia) in response to modern and future ice loss at marine grounding lines in west antarctica. *The Cryosphere*, 16(6):2203–2223, 2022.
- [88] M. Wolstencroft, Z. Shen, T. E. Törnqvist, G. A. Milne, and M. Kulp. Understanding subsidence in the mississippi delta region due to sediment, ice, and ocean loading: Insights from geophysical modeling. *Journal of Geophysical Research: Solid Earth*, 119(4):3838–3856, 2014.
- [89] H. B. Woo, M. P. Panning, P. N. Adams, and A. Dutton. Karst-driven flexural isostasy in north-central florida. *Geochemistry, Geophysics, Geosystems*, 18(9):3327–3339, 2017.
- [90] R. Wood. *General Evolution of Carbonate Reefs*, pages 452–469. Springer Netherlands, Dordrecht, 2011. ISBN 978-90-481-2639-2. doi: 10.1007/978-90-481-2639-2_16. URL https://doi.org/10.1007/978-90-481-2639-2_16.